J. Synchrotron Rad. (1998). **5**, 1227–1234

Energy-Resolving X-ray Fluorescence Detection Using Synthetic Multilayers

K. Zhang,[a]* G. Rosenbaum[b] and G. Bunker[a]

[a]Department of Biological, Chemical and Physical Sciences, Illinois Institute of Technology, Chicago, IL 60439, USA, and [b]Structural Biology Center, Argonne National Laboratory, Argonne, IL 60616, USA. E-mail: ke@biocat1.iit.edu

(*Received 6 December 1996; accepted 11 December 1997*)

The potential of synthetic multilayers for energy-resolving the X-ray fluorescence in X-ray absorption fine structure (XAFS) experiments is discussed. Two detection systems, one using curved multilayers and the other using graded multilayers to select X-ray fluorescence photons, have been designed to cover a wide energy range with a usefully large solid angle. Such a detector will be more advantageous than the barrel-like crystal-array detector because of the unique properties of synthetic multilayers, such as larger horizontal acceptance angles and bandwidth. In addition, the detector should be much simpler to construct and readily accommodates energy changes, especially the detector using graded multilayers. Comparison of the multilayer array detector with conventional detectors, such as ionization chambers and conventional 13-element Ge detectors, shows that the proposed system will be superior, particularly with the increased photon fluxes available from insertion devices and with decreased sample concentration, since this detection system eliminates the 'bad' photons before they enter any X-ray detector. Consequently, the X-ray detector proper for this system does not suffer from the incident-count-rate bottleneck common to current X-ray fluorescence detectors with energy resolution by signal processing. Thus, this new fluorescence detection system will provide tremendous opportunities for XAFS measurements on dilute systems, such as biological systems, at third-generation synchrotron sources.

Keywords: fluorescence detectors; X-ray absorption spectroscopy; synthetic multilayers.

1. Introduction

X-ray fluorescence detection is a commonly used technique in X-ray absorption fine structure (XAFS) applications on dilute systems (Stern & Heald, 1983). In this case the fluorescence signal arising from the absorption of the spectroscopically interesting atoms is only a small part of a large background from coherent and incoherent scattering of the X-ray photons. Statistical fluctuations in the number of scattered background photons are a principal source of noise, and significantly degrade the signal-to-noise ratio in XAFS measurements. Thus, discrimination of the desired X-ray fluorescence against the undesired background is essential for fluorescence detection. The first XAFS fluorescence spectrum was taken by an energy-resolving lithium-drifted germanium detector (Jaklevic *et al.*, 1977). Since that time, various detection schemes have been utilized to optimize X-ray fluorescence detection in dilute systems.

One early approach was to use a crystal analyser array detector made of either pyrolytic graphite (Hastings *et al.*, 1979) or LiF crystals (Marcus *et al.*, 1980) to detect fluorescence in metal alloys and metalloproteins. The detectors, consisting of a crystal array mounted on a barrel-like surface, have superb energy resolution. However, such detectors usually have a very small detection solid angle ($<0.05\pi$ sr) and are only suitable for a narrow energy region because of the need to satisfy the diffraction/focusing conditions. Stern & Heald (1979) demonstrated a combination of low-band-pass filter and Soller-type slits placed before a non-energy-resolving detector, such as an ionization chamber, to suppress the background. The filter reduces the background much more than the signal, and slits block most of the filter fluorescence from entering the detector. This type of detector can provide a large solid

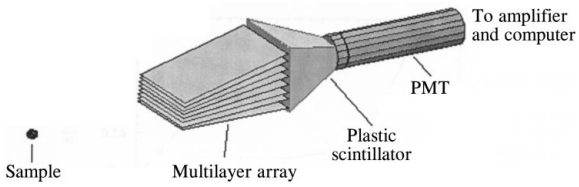

Figure 1
Schematic diagram of the proposed multilayer array detector. Graded or curved multilayers are used to form an analyser array. Shown here is a stack of multilayers which have the same orientation with respect to the line from the point source. The photons selected by the diffraction of the multilayers can be collected using non-energy-resolving detectors, such as scintillation detectors.

angle, but the increase in efficiency is limited primarily by residual filter refluorescence and attenuation of signal counts by the filter. The filter/slit combination is useful in conjunction with conventional Ge and Si energy-dispersive detectors because of their limited maximum count rates.

For very dilute systems, where the background count rate is 20–100 or more times the signal count rate, energy-resolving detectors with reasonable solid angle are most desirable. The Canberra 13-element pure-germanium detector, which has a very good energy resolution (200 eV at 6 keV) and a high total count rate (1×10^6), was designed for such applications (Cramer *et al.*, 1988). The detector has received wide acceptance in measuring fluorescence in dilute systems, in particular biological systems. In addition to the increased efficiency, the detector has the benefit of reducing artifacts caused by intensity variations of the background, which may originate from the diffraction of small ice crystals in frozen solution samples. Indeed, the Ge detector has made a major impact for providing reliable data in biological XAFS applications. The solid-state detector has since improved significantly on two accounts. First, the redesign of the Canberra pre-amplifier and shaping amplifier (model 2101 and 2016) and the advances in digital processing technology (Hubbard *et al.*, 1996) have increased the count rate of the Ge detector three- to fourfold for a single detection channel. Second, larger arrays of detector elements operating at non-cryogenic temperatures, such as the 100-element HgI_2 (Patt *et al.*, 1995) and the 128-element Si (Pullia *et al.*, 1996) detector systems, are being developed. These detectors have an overall count rate exceeding 1×10^6 counts s^{-1}, with a good energy resolution.

Despite its superiority over other fluorescence detectors for dilute systems, the Ge detector suffers from dead-time losses originating from its pulse-counting electronics (Cramer *et al.*, 1988). The absorption spectra can be severely distorted if precautions are not taken (Zhang *et al.*, 1993). More importantly, the maximum count rate of the detector (sum of background and signal counts), determined by the detector dead-time, limits the efficiency of the data collection. Already at bending-magnet beamlines of second-generation radiation sources, such as the NSLS, the available flux often exceeds the detector rate limit. Although the dead-time of the Ge detector can be reduced by replacing the slower pulse-shaping electronics with faster digital pulse-processing systems (Rosenbaum, 1993; Hubbard *et al.*, 1996) and/or by adding more elements/channels to the detector, the problem remains with the ever-increasing photon fluxes at various synchrotron sources in the USA and around the world.

With third-generation synchrotron sources, such as the European Synchrotron Radiation Facility (ESRF) and the Advanced Photon Source (APS) at Argonne National Laboratory, it is expected that the photon flux will increase by a factor of 100–1000 relative to bending-magnet lines. For example, fluxes in a few eV bandwidth from APS undulator A are of the order of 10^{14} photons s^{-1}. These developments provide real opportunities for XAFS applications in determining the structure and time course of a time-resolved reaction, and for even more dilute systems, such as biological membranes and single monolayer protein systems. However, these dramatic increases in photon flux will have little positive effect on XAFS data-collection speed for dilute systems if one is limited to using currently available detector systems. Current integrating detectors, such as fluorescence ion chambers, combined with filters and slits would benefit from increased flux, but they suffer from the same limitations that they have on bending-magnet lines, specifically low efficiency (effective counts/signal counts), which prolongs the experiments and increases the radiation burden on the sample for a given signal-to-noise ratio. Solid-state Ge and Si detectors will have to be operated very inefficiently to avoid detector saturation. The same is true, to a greater or lesser extent, for any detector that accomplishes energy discrimination by processing of detector signals. Only a detector system that removes the unwanted background *before* it reaches the detector electronics can, in our opinion, solve the dilemma of detectors always lagging behind increasing available fluxes. Here we present the concepts for developing energy-resolving detector systems using synthetic multilayers. This type of detector will essentially remove the throughput bottleneck by combining a very high count rate with high data collection efficiency and reasonable solid angle.

2. Rationale and design considerations

Synthetic multilayers are made by depositing alternating layers of two or more kinds of materials, having a significant difference in their indices of refraction in the X-ray wavelength range (Underwood & Barbee, 1981). Multilayers have received much attention for X-ray optics due to their high reflecting power (50–80% or better diffraction efficiency) and large bandwidth (0.005–0.1) (see, for example, Batterman & Bilderback, 1991). The proposed X-ray fluorescence detector will comprise an array of multilayer analyser/detector modules mounted within a device that permits all modules to be rotated simultaneously to the correct Bragg angle for the desired energy. The concept of using multilayers as analysers is essentially the same as using a focusing crystal monochromator array to select the X-ray fluorescence photons (Hastings *et al.*, 1979; Marcus *et al.*, 1980), but with one distinct advantage: the Bragg widths are much wider, making angular alignment and the acceptance angle much larger in the diffraction plane, increasing the acceptance in the plane of the multilayer. The photons selected by diffraction by the multilayers or crystals can be detected using non-energy-dispersive detectors, such as ionization chambers, PIN diodes and scintillation detectors. A schematic of the multilayer array detector is shown in Fig. 1. To simplify the following discussion, the Bragg equation will be used to describe the optical properties of multilayers, although deviations from

this relation occur due to absorption and refraction (Underwood & Barbee, 1981).

In order to accept a single energy from a point source, a multilayer with constant lattice spacing has to be bent to a cylinder of radius R, with

$$R = 2duE/C_\lambda, \tag{1}$$

where d is the layer repetition period (d-spacing) of the multilayer, u is the distance of the center of the multilayer from the source of fluorescence (*i.e.* the sample), E is the fluorescence photon energy, and C_λ = 12397 eV Å. In this curved multilayer case, the selection of the fluorescence energy requires adjustment of radius R and/or distance u in addition to rotating the multilayer to the appropriate Bragg angle. In reality, changing R will be difficult when several tens of multilayer elements are involved, whereas the distance change between detector elements and the source should be much easier to accomplish. Thus, we adopt a fixed-radius curvature in our design for curved multilayer array detectors.

The diffraction condition can also be satisfied in the diffraction plane without bending the multilayers, by grading the lattice spacing instead. For a small Bragg angle (as long as $\cos\theta$ is sufficiently close to 1), the grading ratio is a linear function of position x, and can be written as

$$d(x)/d_0 = 1 + x/u, \tag{2}$$

where d_0 is the minimum d-spacing, $d(x)$ is the d-spacing at position x, and u is the distance of the front edge of the multilayer from the source. It is interesting to note that the grading ratio has no energy dependence. Therefore, a so-graded multilayer will be suitable for the detection of different X-ray fluorescence at a fixed detector–source distance requiring only the adjustment of the Bragg angle.

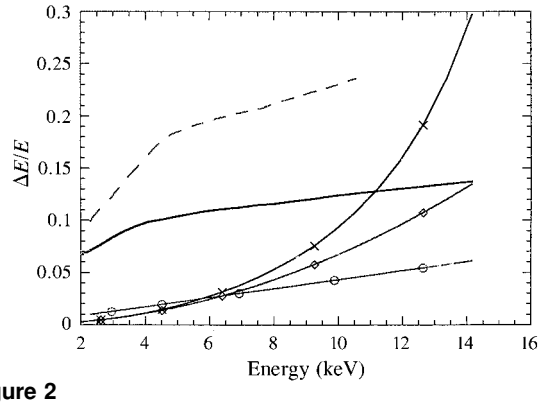

Figure 2
Maximum energy deviation due to a source size of 0.4 mm (diamonds) and object caustic (crosses) under the conditions of $x = 0$ and $s = 0$, respectively. Also plotted here is the maximum deviation due to a source size of 0.4 mm for a graded multilayer (circles). The dimensions and d-spacing used for the calculation can be found in the text. Also plotted here are the energy differences between edge energy and fluorescence energy for $K\alpha$ (solid line) and $L\alpha$ (dashed line) fluorescence of the elements in the periodic table, which are normalized with the fluorescence energies.

For both the curved and graded multilayer detection schemes, the energy deviation caused by the horizontal acceptance angle can be expressed as

$$\Delta E/E = [1/(\cos\varphi)] - 1, \tag{3}$$

where φ is the half horizontal acceptance angle. For a horizontal acceptance angle of 0. 6 rad, $\Delta E/E$ is less than 5%, which is generally adequate for the energy-resolution requirement of a fluorescence detector. This large horizontal acceptance angle is one of the most important advantages of using relatively large d-spacing multilayers. The large horizontal acceptance angle is sufficient to compensate for the small vertical acceptance angle as compared with the crystal analyser array. The use of large pieces of analyser elements will also simplify the design of the array detector.

The energy deviation in the vertical direction for the curved detection scheme is due to the vertical source size and the geometrical aberration of the source (object caustic) caused by the Johann arrangement (Witz, 1969),

$$\Delta E/E = C_{\rm Ed}^2[(s/R - x^2/2R^2)/(1 + xC_{\rm Ed}/R)], \tag{4}$$

where s is the vertical source size, x is the position of the multilayer in the diffraction plane, and $C_{\rm Ed} = 2dE/C_\lambda$. The two terms tend to cancel each other out. The energy deviation due to vertical source size is different for the graded multilayer case,

$$\Delta E/E = 2d_0Es/C_\lambda u. \tag{5}$$

The relative energy deviation of the graded multilayers is a linear function of energy, while that of the curved multilayers is a function of the square of the energy. The maximum relative energy deviation can be estimated for both curved and graded cases using real parameters. In the curved case, this deviation depends on the relative size of the two terms in (4). For $s_{\rm max}$ = 0.4 mm, $x_{\rm max}$ = 50 mm and R = 3100 mm, the two terms in (4) are approximately equal. The maximum (minimum) energy deviation can be evaluated separately for $x = 0$ or $s = 0$. Using d = 20 Å, R = 3100 mm, $s_{\rm max}$ = 0.4 mm and $x_{\rm max}$ = 50 mm, the half-maximum energy deviation caused by the vertical source size ($x = 0$) and by the object caustic ($s = 0$) is plotted in Fig. 2. The energy deviation caused by object caustic is averaged for $x = \pm 50$ mm. For the purpose of comparison, the relative energy differences between the absorption edge and the emission energy for $K\alpha$ and $L\alpha$ fluorescence of the elements in the periodic table are also plotted in the same figure. It can be seen that the energy deviation caused by the vertical beam size of 0.4 mm is less than the corresponding energy difference between fluorescence and emission energies below 14 keV. However, the energy deviation caused by the object caustic increases drastically at higher energies for a 100 mm-long multilayer. This restricts the use of longer multilayers. The maximum deviation can also be evaluated for the case of using graded multilayers. Using d_0 = 20 Å, and u = 150 mm, the energy deviation is also plotted in Fig. 2 for a maximum source size

Table 1
Design characteristics for a curved 40 multilayer array.

The following parameters are used in the calculation. Dimensions of multilayer: 100 mm-long 60–100 mm-wide ladder shape with d = 20 Å. Radius of curvature (Rowland circle), R: 3100 mm. Maximum vertical sample size: 0.4 mm.

Fluorescence energy	Fe $K\alpha$	Zn $K\alpha$
Bragg angle	49 mrad	36 mrad
$\Delta E/E_{max}$ (vertical source)	0.027	0.050
$\Delta E/E_{max}$ (horizontal acceptance)	0.020	0.036
Sample–detector distance	150 mm	111 mm
Vertical angular acceptance	32 mrad	32 mrad
Solid angle (40 array)	0.52 sr	0.64 sr

of 0.4 mm. The maximum energy deviations stay well below the energy difference of the $K\alpha$ fluorescence.

One of the most important design concerns is the detection solid angle which is determined in part by the vertical acceptance angle, $\Delta\alpha$, of the detector elements. In the curved case,

$$\Delta\alpha = x/R, \tag{6}$$

where x is the length of the multilayer. For the graded multilayer,

$$\Delta\alpha = C_\lambda x/[2d_0E(x+u)]. \tag{7}$$

The vertical acceptance angle in the curved case is independent of the fluorescence energy. Thus, the solid-angle variation in this case depends only on the horizontal acceptance angle, which increases with the fluorescence energy. The vertical acceptance angle in the graded case is inversely proportional to the energy. Since the horizontal acceptance angle is constant in this case, the solid angle will decrease with the increase of the fluorescence energy.

Generally speaking, the constant vertical acceptance angle of the curved multilayer detector design permits compact packing of multilayer elements, resulting in a larger detection solid angle than the graded case, especially in the higher-energy region. However, the increased solid angle degrades the energy resolution due to decreased detector–sample distances at higher energies. Unlike the graded multilayer detector, which has a fixed sample–detector distance, the sample–detector distance has to be changed when changing fluorescence energy for the curved multilayer detector in order to satisfy diffraction conditions with a fixed radius R of a Rowland circle. The selection of curved or graded multilayer detectors depends on the energy region to be covered, the energy resolution required, other design considerations, and cost factors. Table 1 lists design characteristics for a curved multilayer array detector with 40 elements to cover the energy range 5–9 keV ($K\alpha$ energies of 3d transition-metal elements V through Zn). We select 100 mm-long by 60–100 mm-wide multilayers of trapezoid shape with a d-spacing of 20 Å. The multilayers have a design radius of curvature of 3100 mm. The collection solid angle is approximately 0.52 sr at the Fe $K\alpha$ fluorescence energy, and 0.64 for Zn.

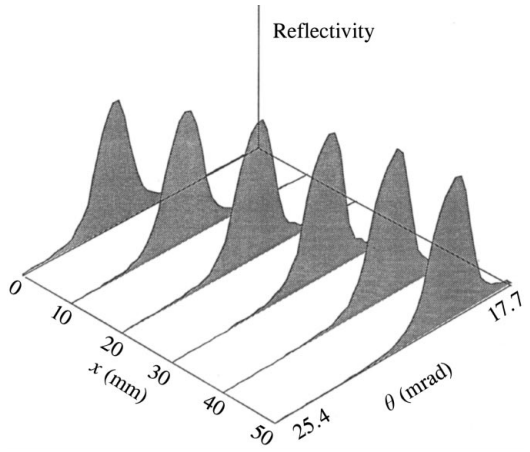

Figure 3
Rocking curve at various positions of the graded multilayer tested at the synchrotron beamline, where x is the position on the multilayer and θ is the incident angle of the X-ray beam.

The relations described previously can be used to aid in the design of multilayer detectors for use at different energy ranges. In the low-energy range (2–4 keV, for example), a larger vertical acceptance angle can be readily achieved for individual detector elements [equations (6) and (7)]. However, the Bragg angle is still so small that the equations described above are still valid. Thus, the detectors to cover this energy region can be built with fewer elements and/or a larger solid angle. Conversely, small d-spacing multilayers are needed for detection in the high-energy region (higher than 15 keV) to ensure good energy resolution and reasonable solid angle. However, such multilayers combining small d-spacing and small layer deviation required for high-energy applications may be technically difficult to make. Thus, single crystals might be preferable to synthetic multilayers in this case.

A graded multilayer has been tested at beamline X9-B of NSLS. The size of the multilayer is 3 cm wide and 6 cm long, and is designed to have a linear d-spacing change over its length. Fig. 3 shows the rocking curve at various positions on the multilayer. The d-spacing change is fairly linear from 46 to 52 Å, except for the end points. The reflectivity is about 75%, and the bandwidth (full width at half-maximum; FWHM) is about 4% at 8 keV. The test shows that the technology for making the multilayers required for the detector is available (Gutman *et al.*, 1992).

The performance of the detector depends primarily on the rejection of the elastically scattered background of the multilayer, which is determined by the detailed shape of the reflectance curve, the shift and the broadening of this curve due to vertical source size and horizontal acceptance angle. However, the reflectance curve is the most important factor determining the performance of the detector provided that the maximum energy deviation due to geometry factors remains small as in the design model (Table 1). Fig. 4 shows one of the experimental reflectance curves (solid) in the energy range of copper $K\alpha$ fluorescence, compared with the response of the Canberra 13-element Ge detector

normalized to the peak height of the reflectance curve. From the reflectance curve, the ratio in reflectance at 8 keV (Cu $K\alpha$) and 9 keV (Cu K-edge) is more than 100, while for the Ge detector the ratio in response to photons at the two different energies is only 60. These compare with FWHM of 380 eV for the multilayer reflectance curve and 330 eV for the response of the Ge detector. The relatively flat top and sharp drop from the center of the reflectance is a virtue of its applications in X-ray fluorescence detection.

The reflectance curve of multilayers can be calculated accurately from Fresnel equations (Underwood & Barbee, 1981). The calculated curve for the tested multilayer is compared in Fig. 4. Good agreement can be obtained by adding a small Gaussian type of roughness on the interfaces. Plotted in Fig. 5 are the calculated maximum reflectivity and FWHM of the reflectance curve, as a function of tungsten thickness, for two W/Si multilayers with 20 and 40 Å d-spacing. It shows that the shape of the reflectance curve can be controlled during the multilayer deposition. With the decrease of d-spacing, the reflectance curve becomes narrower while the peak reflectivity remains the same. Thus, it is expected that the multilayer array detector can be made with a much higher degree of background rejection than the Ge detector if the broadening due to geometrical effects can be restricted.

3. Discussion and comparison

The proposed detector has more advantages than the barrel crystal monochromator array detector (Hastings *et al.*, 1979; Marcus *et al.*, 1980). First, the major advantages of the multilayer detectors originate from the large horizontal acceptance angle of the multilayers. This allows the use of large pieces of multilayers that are flat in the direction perpendicular to the diffraction plane, resulting in a large solid angle and simplified detector design. It also permits the use of the geometry in which the footprint of the beam on the sample is a line, rather than a point, as is required for the barrel-like array detectors. By the same token, fluorescence energy changes can be achieved for the graded multilayer detector by simply rotating the detector elements, and by a combined translation and rotation for the curved multilayer detector. Second, due to the large bandwidth and reflectivity of the multilayers, the array detector is efficient, and, for the same reason, is more tolerant to misalignment problems. Third, since the deposition of the multilayers is a controllable process, the detector elements can be tailored to provide desirable energy selectivity for different applications.

A detailed comparison can be made between the multilayer array detector and the conventional fluorescence detectors. The effective signal count rate in the fluorescence detection can be expressed as

$$N_{\rm eff} = N_s^2/(N_s + N_b), \tag{8}$$

where N_s and N_b are the signal and background count rates, respectively. In a dilute system, where the concentration of the atoms of spectroscopic interest is in the range of a few hundred p.p.m. to several tens of p.p.m., the background-to-signal ratio can be as high as 20:1 to 100:1. As a result, the effective signal count will be degraded many times in such applications using non-energy-resolving detectors. Thus, energy-resolving detectors, which eliminate background counts, are most desirable.

In the non-energy-resolving fluorescence detector, the background can be suppressed with a filter/Soller-type slits

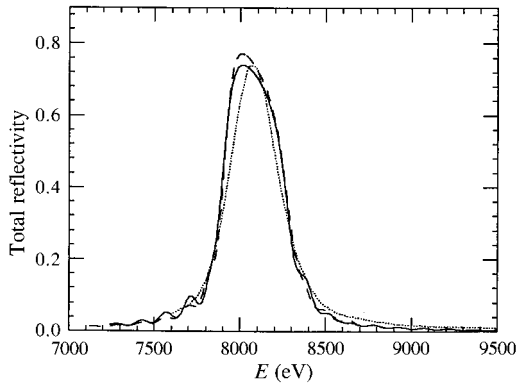

Figure 4
The experimental reflectance curve (solid line) of the multilayer compared with the reflectance curve (dashed line) calculated by solving Fresnel equations. A Gaussian distribution with a 3.8 Å width is used to take into account the interface roughness. Also plotted here is the response of the 13-element Ge detector (Canberra Gl 0110) (dotted line) *versus* incident photon energy. The single-channel analyser (model 2031) was set to a center energy corresponding to 8.07 keV and an energy window corresponding to 8 eV. A model 2020 spectroscopic amplifier was used, with a shaping time of 1 μs. The incident beam had a bandwidth of a few eV.

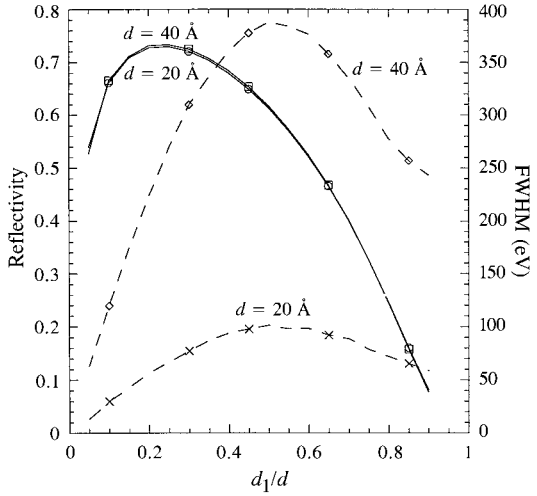

Figure 5
Calculated peak reflectivity (solid line) and bandwidth (dashed line) at 6.3 keV for W/Si multilayers with 20 and 40 Å d-spacing as a function of the fraction of W thickness. The results were obtained under saturation conditions.

Table 2
Estimated solid angle and effective counts of fluorescence detection for a 1 m*M* iron solution sample.

The assumptions used in generating the table are as follows. Optimized filter/slits with $Q = 5$, $\eta = 0.02$; count-rate limit of the Ge detector = 200 K per channel; sample thickness = 1 mm; absorption of windows and air reduce the signal and background by 60%; B/S ratio is 40 for small solid angle and 60 for large solid angle. The parameters in Table 1 are used for the multilayer array detector.

	Unfocused beam (2×10^{10})			Focused beam (2×10^{11})		
Detectors	Filter/slits $\Delta\mu x$	Solid angle (sr)	Effective count rate	Filter/slits $\Delta\mu x$	Solid angle (sr)	Effective count rate
Ge detector 13-element	Yes 0.8	0.3	1.4×10^5	Yes 3.2	0.3	7.8×10^5
40 curved multilayer array	None –	0.5	2.9×10^5	None –	0.5	2.9×10^6
Ion chamber	Yes 3.3	1.2	4.8×10^4	Yes 3.3	1.2	4.8×10^5

combination (Stern & Heald, 1979). With this combination, the effective signal count can be calculated as

$$N_{\rm eff}/N_s = \exp[-\Delta\mu x(Q-1)^{-1}] \times \{1 + ((N_b/N_s)\exp(-\Delta\mu x) \times [1 + \eta(\exp\{\Delta\mu x[Q/(Q-1)]\} - 1)])\}^{-1}. \quad (9)$$

Here, Q equals the ratio of the absorption of the filter above the absorption edge to the absorption at the fluorescence energy, which is a measure of the quality of the filter (usually in the range 3–6 for the filters made of 3*d* transition metals), $\Delta\mu x$ is the difference between the two absorptions, and η is the fraction of photons absorbed by the filter that still find a way into the detector in the form of filter refluorescence. The value of η is approximately 0.15 if no slits are used, and 0.02 if good slits are used. The thickness of an optimized filter can be calculated according to (9) given the quality of the filter and the slits, as well as the background-to-signal ratio. In the dilute limit, in which the background is much larger than the signal (for example, approximately 100-fold), the optimized filter thickness satisfies a simple relation,

$$\Delta\mu x = [(Q-1)/Q]\ln[(Q-2)(1-\eta)/2\eta]. \quad (10)$$

Taking $Q = 5$ and $\eta = 0.02$, the thickness $\Delta\mu x$ of the optimized filter is 3.4 in the dilute limit, and the increase of the effective signal counts, with respect to the non-filter case, is 5.4 times.

The filter and Soller slits can also be used to increase the signal counts for the Ge detector. For a flux-limited detector system at high dilution limits, effective signal counts are maximized if the ratio of signal counts to background counts is maximized. This optimization is achieved if

$$\Delta\mu x = [(Q-1)/Q]\ln[(Q-1)(1-\eta)/\eta]. \quad (11)$$

For $Q = 5$ and $\eta = 0.02$, $\Delta\mu x$ of the optimized filter is 4.1, and the signal-to-background ratio increases by 14 times. With this optimized filter and slits, the detector–sample distance can be adjusted to bring the total counts (signal plus background) within the near linear response region of the detector. Thus the most important parameter determining the efficiency of the Ge detector is the maximum count rate of the pulse-processing system. We take this to be 2×10^5 per channel, comparable with the currently available Canberra system (spectroscopy amplifier model 2016 with 0.125 µs shaping time).

In reality, the 14-times increase of signal to background cannot be fully translated to the increase of efficiency for the Ge detector. Since the fluorescence energy is closer to the filter refluorescence energy than to the X-ray energy, a large portion of the filter refluorescence photons are counted during measurements. For example, the Cu $K\alpha$ fluorescence energy is approximately 570 eV from the $K\alpha$ and 200 eV from the $K\beta$ refluorescence energy of an Ni filter, compared with 900 eV from the Cu *K*-absorption edge. The background rejection rate in this case will drop substantially when using a filter due to the long tail of the response curve for the Ge detector (Fig. 4). However, this effect is not included directly in the current detector performance evaluation.

When the photon flux is $\sim 10^{10}$ photons s^{-1}, the limiting factor of the Ge detector is its solid angle. Placing the Ge detector 6–7 cm away from the sample will result in a solid angle of 0.3 sr. The detection solid angle for a non-energy-resolving detector is estimated to be 1.2 sr when filter and Soller slits are used. The larger the solid angle, the higher the background-to-signal ratio will be when collecting data away from the direction in the horizontal plane perpendicular to the beam direction. This is due to the angular dependence of the scattering distribution. This angular-dependent term limits the increase of the effective signal count at larger solid angles. For example, the doubling of the solid angle from 1.2 to 2.4 sr for a dilute sample increases the effective signal counts by less than 20%.

Comparisons can be readily made between the three different detectors, namely the 13-element Ge detector, the multilayer array detector (using the design model shown in Table 1), and a fluorescence ionization chamber. To simplify the comparisons, we assume perfect background rejection for the energy-resolving detectors, namely all background photons are rejected by the detectors. The comparison is first made on a bending-magnet beamline, such as X9-B of NSLS which can be focused vertically and horizontally. With a 1 mm-thick solution sample of 1 m*M* iron concentration, the absorption of the X-ray by the

metal ions can be calculated and the fluorescence counts due to the absorption can be estimated. Taking into account that the background-to-signal ratio for such a sample can be 30–40 times for a small solid angle (0.3–0.4 sr) and more than 100 times for a large solid angle (1.2 sr), and compensating for the absorption by various windows in a real XAFS experiment, the signal counts collected by these detectors can be estimated according to various configurations.

The results of the comparison are summarized in Table 2. It can be seen that the performance of the Ge detector is several times better than that of the ionization chamber with optimized filter and slits under unfocused operation, while the performance of the multilayer array detector is approximately two times better than that of the Ge detector. Under focused operation, however, the performance of the Ge detector is approximately the same as that of the ionization chamber, while that of the multilayer array detector is several times better. Generally speaking, with the increase of the photon flux the efficiency advantage of the Ge detector over the non-energy-resolving detector disappears and reverses due to the decreased effective detection solid angle. In this case, the performance of the multilayer detector is six to seven times better than both of them.

The proposed multilayer array detector will be many times better than those 'conventional' X-ray fluorescence detectors when measuring more dilute systems at the APS, where a factor of 100–1000 flux increase is expected. The increase in efficiency of the multilayer array detector can be further estimated under the high-flux and high-dilution conditions using the same detection solid angle given in the previous example for both the multilayer array detector (0.5 sr) and the ionization chamber (1.2 sr), and a homogeneous background-to-signal ratio of 200:1 (for a sub-mM sample). The signal counts for both the multilayer array detector and the non-energy-resolving detectors will increase linearly with the increase of the photon flux. Under this dilute limit, the optimized filter/slits (with $Q = 5$ and $\eta = 0.02$) will increase the effective signal counts for the ionization chamber by 5.4 times. Under high-flux conditions, the efficiency of the 13-element Ge detector will be determined by the maximum count rate of the detector (2.6×10^6 with the fast pulse-processing system). A factor of 14 efficiency increase of the Ge detector can be obtained by optimizing the signal-to-background ratio with filter/slits. The estimated signal counts under various detection schemes are plotted in Fig. 6 as a function of photon flux on the sample. Under the high-flux limit, the efficiency of the Ge detector, defined as the collection of effective signal counts for a given sample, remains unchanged with the increase of the photon flux. At this metal concentration, the advantage of the multilayer array detector over the non-energy-resolving detector becomes more evident.

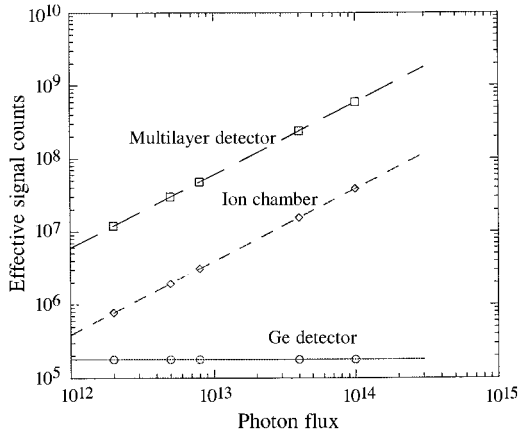

Figure 6
Projected signal counts as a function of photon flux for various detectors. The estimations are based on high-flux (more than 10^{12}) and high-dilution (200:1 background-to-signal ratio) conditions. Optimized filter/slits are used for the Ge detector and the ionization chamber. The distribution of the scattered background is assumed to be homogeneous.

To summarize, the detection of X-ray fluorescence using synthetic multilayers has been proposed. We have shown that such detectors can be built with a very high count rate, superb energy resolution, yet a reasonable solid angle. The simplified comparisons show that the multilayer detector will be superior to the currently used detectors (energy-resolving and non-resolving) for sensitive fluorescence detection with a high photon flux. Thus, it is desirable for the fluorescence detection for very dilute systems and at third-generation synchrotron sources. The construction of the multilayer detectors discussed in this paper is being actively pursued. The design of the detectors and detailed performance simulation and measurements will be discussed in a forthcoming paper.

The research reported here was supported by NSF grant BIR-9419635. We appreciate the support of the staff of beamlines X9-B and X18-B, and the National Synchrotron Light Source, which is supported by DOE.

References

Batterman, B. W. & Bilderback, D. H. (1991). *Handbook on Synchrotron Radiation*, Vol. 3, edited by G. S. Brown & D. E. Moncton, p. 105. Amsterdam: Elsevier.
Cramer, S. P., Tench, O., Yocum, M. & George, G. N. (1988). *Nucl. Instrum. Methods*, A**266**, 586–591.
Gutman, G., Keem, J., Parker, K., Wood, J. L., Watts, R. & Tarrio, C. (1992). *Proc. SPIE*, **1742**, P373–P383.
Hastings, J. B., Eisenberger, P., Lengeler, B. & Perlman, M. L. (1979). *Phys. Rev. Lett.* **43**, 1807–1810.
Hubbard, B., Warburton, W. K. & Zhou, C. Z. (1996). *Rev. Sci. Instrum.* **67**, 1–3 (CD-ROM).
Jaklevic, J., Kirby, L. A., Klein, M. P., Robertson, A. S., Brown, G. S. & Eisenberger, P. (1977). *Solid State Commun.* **33**, 679–682.
Marcus, M., Powers, L. S., Storm, A. R., Kincaid, B. M. & Chance, B. (1980). *Rev. Sci. Instrum.* **51**, 1023–1029.
Patt, B. E., Iwanczyk, J. S., Szezebiot, R., Maculewiez, G., Wang, W., Wang, Y. J., Hedman, B., Hodgson, K. O. & Cox, A. D. (1995). *IEEE Trans. Nucl. Sci.* **42**, 558–564.
Pullia, A., Furenlid, L., Kraner, H. W., Bertuccio, G., Pietraski, P. J. & Siddons, D. P. (1996). *Rev. Sci. Instrum.* **67**, 1–8.

Rosenbaum, G. (1993). Personal communications.
Stern, E. A. & Heald, S. M. (1979). *Rev. Sci. Instrum.* **50**, 1579–1585.
Stern, E. A. & Heald, S. M. (1983). *Handbook on Synchrotron Radiation*, Vol. 1, edited by E. E. Koch, p. 955. Amsterdam: North-Holland.
Underwood, J. H. & Barbee, T. W. Jr (1981). *Low Energy Diagnostics, AIP Conference Proceedings*, Vol. 75, edited by D. T. Attwood & B. I. Henke, pp. 170–178. New York: AIP.
Witz, J. (1969). *Acta Cryst.* A**25**, 30–43.
Zhang, K., Rosenbaum, G. & Bunker, G. (1993). *Jpn. J. Appl. Phys. Suppl.* **32**, 147–149.